Journal of Materials Chemistry A

Thermoelectric Properties of Mn-doped Mg-Sb Single Crystals

Journal:	*Journal of Materials Chemistry A*
Manuscript ID:	TA-ART-05-2014-002386.R1
Article Type:	Paper
Date Submitted by the Author:	03-Jun-2014

Complete List of Authors:	Kim, Soo Hyun; Sogang University, Physics Kim, Chung Man; Sogang University, Physics Hong, Yang-Ki; The university of alabama, electrical and computer engineering Onimaru, T; Hiroshima University, ADSM, Department of Quantum Matter Suekuni, Koichiro; Hiroshima University, ADSM, Department of Quantum Matter Toshiro, Takabatake; Hiroshima University, ADSM, Department of Quantum Matter Jung, Myung-Hwa; Sogang University, Physics

Thermoelectric Properties of Mn-doped Mg-Sb Single Crystals

Soohyun Kim,[a] Chungman Kim,[a] Yang-Ki Hong,[b] Takahiro Onimaru,[c] Koichiro Suekuni,[c] Toshiro Takabatake,[c] and Myung-Haw Jung[a,*]

[a]Department of Physics, Sogang University, Seoul 121-742, South Korea
[b]Department of Electrical and Computer Engineering, University of Alabama, Tuscaloosa, Alabama 35487, USA
[c]Department of Quantum Matter, ADSM, Hiroshima University, Kagamiyama, Higashi-Hiroshima 739-8530, Japan

Abstract

We have grown $Mg_{3-x}Mn_xSb_2$ (x = 0, 0.3, and 0.4) single crystals by the vertical Bridgman method to investigate the effects of Mn substitution on thermoelectric properties of Mg_3Sb_2. The grown crystals were single phased and c-axis oriented with the trigonal crystal structure of inverse α-La_2O_3 type. The Seebeck coefficient (S), electrical resistivity (ρ), and thermal conductivity (κ) were measured at various temperatures ranging from 4 to 500 K. The electrical resistivity at 500 K decreased to 0.20 Ωcm for x = 0.3 and to 0.16 Ωcm for x = 0.4 from 2.30 Ωcm of Mg_3Sb_2 (x = 0), but the thermal conductivity was 1.04 W/mK for both x = 0 and 0.4. The Seebeck coefficient became negative when Mn was substituted for Mg, but the absolute value remained almost the same as that for x = 0 in the temperature range between 5 and 600 K. The power factor for x = 0.4 has a large maximum of 370 $\mu W/mK^2$ at 130 K. As a result, the thermoelectric figure of merit for Mn-substituted Mg_3Sb_2 is more than one order of magnitude higher than that for pure Mg_3Sb_2 (x = 0).

Key words: Thermoelectrics, Zintl phase, Mg_3Sb_2

* Corresponding author: Tel. +82 2 705 8828, mhjung@sogang.ac.kr

1. Introduction

Thermoelectric efficiency of a given material is determined by the figure of merit, ZT (= $S^2T/\rho\kappa$), where S is the Seebeck coefficient, ρ is the electrical resistivity, κ is the thermal conductivity, and T is the temperature [1,2]. The Seebeck coefficient is large for semiconductors with low carrier concentration, and the electrical resistivity is low for metals with high carrier concentration. Therefore, the thermoelectric power factor (= S^2/ρ) can be maximized between metallic and semiconducting properties. It has been known that a narrow-gap band structure of semiconductors favors thermoelectric effects rather than the gapless band structure of metals [3,4]. Further, the ZT can be optimized by adjusting two modes of thermal conductivity: Phonons are responsible for lattice thermal conductivity and electrons for electronic thermal conductivity [5,6]. Then the thermal conductivity of thermoelectric material has two different components; electron- and phonon-based conductivities (κ_{el} and κ_{ph}, respectively). The κ_{el} is lower than κ_{ph} for semiconductors, and the higher electrical conductivity (σ) gives the higher κ_{el}, thereby possibly decoupling κ_{ph} from σ (= $1/\rho$). Therefore, the κ_{ph} needs to be minimized to achieve high ZT. This suggests that the ZT can be controllable by engineering κ_{ph}.

With regard to the electrical conductivity σ (= $ne^2\tau/m$) of metal, where n is the charge carrier density, e is the charge per carrier, τ is the carrier mean free time between scattering events, and m is the carrier mass, the electrical conductivity is utterly controlled by the carrier mean free time (τ). The electrical conductivity of metals decreases with increasing temperature. This is because the τ decreases as the temperature increases. On the other hand, the electrical conductivity generally increases with temperature for semiconductors due to an increase in n with temperature. Most Zintl phase compounds are valence balanced and poor conductors or semiconductors, which have been intensively studied as potentially high ZT thermoelectric materials [7,8]. Both ionic and covalent bonds need to coexist in the Zintl phase. Mg_3Sb_2 has the Zintl phase structure, and is composed of $(Mg_2Sb_2)^{2-}$ framework and intercalated Mg^{2+} cation layer. The Mg occupies either the tetrahedral site of $(Mg_2Sb_2)^{2-}$ or octahedral site of Mg^{2+}. The covalent bonding of polyanion enhances the mobility of the charge carriers. However, Mg_3Sb_2 has low mobility because of strong polar covalent bonding in the $(Mg_2Sb_2)^{2-}$ framework [7]. Very few studies on polycrystalline and nanocrystalline Mg_3Sb_2 were reported [9-12], but to the best of our knowledge, no study on Mn-substituted Mg-Sb single-crystalline is reported. Kajikawa *et al*., [9] reported ZT = 0.55 at 660 K and Condron *et al*., [10] reported ZT = 0.21 at 875 K for polycrystalline Mg_3Sb_2. However, extremely low ZT of 5.56×10^{-4} at 300 K was reported for Zn-substituted Mg_3Sb_2 [11] and 0.34×10^{-4} for nanocrystalline Mg_3Sb_2 [12]. These different measured ZT values can be explained by microstructure evolution and grain boundary structure [10-12]. The thermal conductivity is low for the nanocrystalline Mg_3Sb_2, but the electrical resistivity is high. Therefore, a low ZT value is expected for the nanocrystalline Mg_3Sb_2. This is because more grain boundary scatterings occur in polycrystalline Mg_3Sb_2. The thermoelectric

properties can be improved in the single crystal form due to the less grain boundary scattering. And also, we try to enhance the electronic transport properties by introducing Mn atoms into Mg_3Sb_2 because the Mn atoms substituted for Mg in the polyanion $(Mg_2Sb_2)^{2-}$ layer can weaken the polar covalent bonding and thereby increase the carrier mobility. In this paper, we report the thermoelectric properties of single crystalline Mg_3Sb_2 and Mn-substituted Mg_3Sb_2, (i.e., $Mg_{3-x}Mn_xSb_2$ with x = 0, 0.3, and 0.4). The figure of merit is compared to that of their polycrystalline counterparts, and interpreted in terms of grain boundary contribution.

2. Experimental

Single crystalline $Mg_{3-x}Mn_xSb_2$ with x = 0, 0.3, and 0.4 were grown by the vertical Bridgman method from mixtures of Mg (99.99%), Mn (99.999%), and Sb (99.999%). A pre-baked and cleaned Mo crucible containing the nominal Mg-Mn-Sb mixture with 0.5 mole Mg excess was sealed by arc melting under Ar atmosphere, and then was heated up to 800 ^oC at 100 ^oC/h rate and kept for 24 h. After homogenizing the mixture at 800 ^oC, the crucible was cooled to room temperature slowly over a total of ~130 h while rotating the crucible at 5 revolutions per minute (rpm). The crystal structure was analyzed by x-ray diffraction using a Rigaku DMAX 2500 diffractometer equipped with CuKα radiation (λ = 1.5406 Å). The physical properties were determined by scanning electron microscopy (SEM, JSM-6700F) and x-ray photoelectron spectroscopy (XPS, SIGMA PROBE). The chemical composition of the grown crystals was measured by electron probe microanalyzer (EPMA, JXA-8900R). We measured the electrical resistivity (ρ), the Seebeck coefficient (S), and thermal conductivity (κ) at various temperatures ranging from 4 to 500 K. Since the grown single crystals were well-cleaved in parallel to the *ab* plane, we performed all the measurements in the plane. A four-point probe with a GM refrigerator was used to measure ρ. To measure the S, we used two different techniques; a slowly varying T-gradient technique from 5 to 300 K and commercial MMR Technologies system from 300 to 600 K. The κ was measured using a steady-state method with a cryostat at temperatures between 5 and 300 K. By the laser flash method, the thermal diffusivity D was measured for the temperature range from 300 to 600 K in vacuum, then the κ could be obtained by $\kappa = DC_pM$, where C_p is the specific heat and M is the mass density. Also, we carried out the Hall measurements using the dc technique at a constant magnetic field of 12 kOe to obtain carrier concentration.

3. Results and discussion

Fig. 1 (a) and (b) show the powder and single crystal x-ray diffraction (XRD) patterns for $Mg_{3-x}Mn_xSb_2$ (x = 0, 0.3, and 0.4), respectively. Single crystals were ground for powder XRD measurement. All diffraction peaks are well indexed with the reported structure of inverse α-La_2O_3 structure-type [9-

14]. The obtained lattice parameters are a = 4.55(6) Å and c = 7.22(4) Å. Mn-substituted Mg_3Sb_2 crystals show the same XRD patterns as the pure Mg_3Sb_2, and the shift of the peak positions is unnoticeable. Therefore, the change in lattice parameters is negligible with Mn substitution. As shown in Fig. 1 (c), the crystals are well-cleaved in parallel to the *ab* plane, and are shiny and flat. Single crystal XRD patterns were taken from the shiny and flat surface, which is the *ab* plane. Thus, the single-crystal diffraction peaks are well labeled with (*00l*) indices as shown in Fig. 1 (b). It is noted that since the melting point of Mn is higher than the boiling point of Mg, the solubility of Mn in Mg-Sb is limited. This limits stoichiometric composition range for $Mg_{3-x}Mn_xSb_2$. By using the electron probe microanalyzer (EPMA), we obtained the actual composition of Mn, that is 0.2 and 0.3 even though the nominal Mn composition was x = 0.3 and 0.4. The scanning electron microscopy (SEM) image in Fig. 1 (d) shows that $Mg_{3-x}Mn_xSb_2$ crystals are homogeneous in phase. Furthermore, in order to identify the valence state of substituted Mn cation, we have taken the x-ray photoelectron spectroscopy (XPS) spectra as shown in Fig. 2. It is known that the binding energy of 640.8 ± 0.3 eV comes from $Mn^{2+}(2p_{3/2})$ and 641.8 ± 0.1 eV from $Mn^{3+}(2p_{3/2})$ [15,16]. Even though the difference in their binding energies is small, we can fit the XPS spectra with two Gaussian functions from $Mn^{2+}(2p_{3/2})$ and $Mn^{3+}(2p_{3/2})$ contributions. As shown in Fig. 2, for x = 0.3 the Mn^{2+} peak (red line) is relatively stronger than the Mn^{3+} peak (blue line), and for x = 0.4 the Mn^{3+} peak is stronger than the Mn^{2+} peak. The sum of two Gaussian functions (green line) well fits the experimental data. This means that the more Mn substitution gives more stable Mn^{3+} states instead of Mn^{2+}. Then, we can expect an increase of n-type carriers with the substitution of Mn.

Fig. 3 shows the temperature dependence of electrical resistivity for $Mg_{3-x}Mn_xSb_2$ (x = 0, 0.3, and 0.4). The Mg_3Sb_2 (x = 0) single crystal possesses 2.52 Ω cm of resistivity at room temperature, which is lower than the resistivity reported for polycrystalline or nanocrystalline Mg_3Sb_2 [11,12]. However, the electrical resistivity is still high compared to other promising thermoelectric materials. This is because the strong polar covalent bonding of $(Mg_2Sb_2)^{2-}$ polyanion limits carrier mobility. In Zintl phase compounds, the carrier mobility is governed by polyanionic bonding. However, the substitution of Mn for Mg sites of Mg_3Sb_2 crystal causes the polyanionic polar covalent bonding to convert to covalent bonding, thereby enhancing carrier mobility. Therefore, the covalent bonding in Zintl phase compounds leads to lower electrical resistivity as compared to polyanionic polar covalent bonding. The measured electrical resistivity of $Mg_{3-x}Mn_xSb_2$ (x = 0.4) is 0.09 Ω cm at room temperature, which is almost 30 times lower than that of Mg_3Sb_2 (x = 0). With increasing temperature, the electrical resistivity decreases for Mg_3Sb_2 (x = 0), but increases for $Mg_{3-x}Mn_xSb_2$ (x = 0.3 and 0.4). This suggests that the substitution of Mn for Mg changes semiconducting behavior of Mg_3Sb_2 (x = 0) to metallic behavior. There are two possible explanations for this change. One is an increase in carrier concentration with Mn substitution. Therefore, we have performed the Hall measurements at room temperature to determine carrier concentration. The measured carrier concentrations were 2.2×10^{17} cm^{-3}, 9.0×10^{17} cm^{-3}, and 13.3×10^{17} cm^{-3} for x = 0, 0.3, and 0.4, respectively. The carrier concentration remarkably increases with x. Further the carrier type changes from p-type in Mg_3Sb_2 (x

= 0) to be n-type in $Mg_{3-x}Mn_xSb_2$ (x = 0.3 and 0.4). It is noted that the valence of Mn can be either divalent (Mn^{2+}) or trivalent (Mn^{3+}), whereas Mg holds a divalent state (Mg^{2+}). As aforementioned, it was confirmed by XPS results that Mn^{2+} and Mn^{3+} cations coexist. Accordingly, the substitution of Mn for Mg provides excess electrons in $Mg_{3-x}Mn_xSb_2$, thereby increasing carrier concentration. This results in lowering the electrical resistivity. The other explanation can be made by an increase of carrier mobility with Mn substitution. As aforementioned, Mg_3Sb_2 with the structure of Zintl phase has strong polar covalent bonding, which decreases the carrier mobility [7]. When Mn is substituted for Mg, the polar covalent bonding of Mg_3Sb_2 (x = 0) becomes weak. Therefore, the weakened polar covalent bonding enhances the mobility, consequently lowering electrical resistivity. To confirm this, we have evaluated the carrier mobility at room temperature from the carrier concentration and electric resistivity data. The evaluated carrier mobility was 11.25 cm^2/Vs, 49.24 cm^2/Vs, and 53.91 cm^2/Vs for x = 0, 0.3, and 0.4, respectively. The carrier mobility increases about 340% by substituting Mn for Mg. This result suggests that the polar covalent bonding of polyanion $(Mg_2Sb_2)^{2-}$ is weakened or destroyed when Mn substitutes for Mg in the tetrahedral site of polyanion framework rather than in the octahedral site of Mg cation layer. Consequently, the electrical resistivity decreases with the substitution of Mn for Mg. The schematic crystallographic structure of $Mg_{3-x}Mn_xSb_2$ is shown in the inset of Fig. 3.

Fig. 4 shows the temperature dependence of Seebeck coefficient for $Mg_{3-x}Mn_xSb_2$ (x = 0, 0.3, and 0.4). The Seebeck coefficient is positive and large for x = 0, but becomes negative value when Mn substituted for Mg. These results are in good agreement with our Hall measurement results, which show that the carrier type changes from p-type to be n-type with Mn substitution for Mg. The Seebeck coefficient for x = 0 is 591 μV/K at 300 K, which is higher than polycrystalline Mg_3Sb_2 [9-11] but lower than nanocrystalline Mg_3Sb_2 [12]. However, the measured value for x = 0.4 is -496 μV/K at 300 K, the absolute value of which is unexpectedly high as compared to other substituted materials [11]. Therefore, we have tried to understand this through the following analysis. The maximum Seedbeck coefficient (S_{max}) is given by the relation $S_{max} \sim E_g/2eT_{max}$ [17], where S_{max} is the maximum value of the Seebeck coefficient, E_g is the band gap, and T_{max} is the temperature at the S_{max}. The E_g was estimated to be 0.8 eV from the Seebeck coefficient versus temperature plot (T_{max} = 580 and 570 K for x = 0 and 0.3), and is close to the band gap of Mg_3Sb_2 measured by an optical technique [18,19]. This means that the substitution of Mn for Mg of Mg_3Sb_2 is not sufficiently effective in changing the band gap. Therefore, the Seebeck coefficient of $Mg_{3-x}Mn_xSb_2$ (x = 0.4) remains high.

In order to assess the ability of Mg-Mn-Sb crystals to produce useful electric power, we have calculated the power factor (S^2/ρ) from the measured electrical resistivity (ρ) and Seebeck coefficient (S). Fig. 5 shows the temperature dependence of the power factor for $Mg_{3-x}Mn_xSb_2$ (x = 0, 0.3, and 0.4). The power factor for x = 0.3 and 0.4 increases up to 150 K and then decreases, while the power factor for x = 0 monotonically increases with the temperature. The power factor of single crystalline Mg_3Sb_2 is about 14 $\mu W/mK^2$ at room temperature, and is close to that of polycrystalline Mg_3Sb_2 [11], but is much higher than nanocrystalline Mg_3Sb_2 [12]. It is noted that the power factor becomes the

same at 500 K for both $Mg_{3-x}Mn_xSb_2$ (x = 0.3 and 0.4) single crystals. It can be concluded that the power factor is increased with the substitution of Mn for Mg of Mg_3Sb_2 due to remarkable decrease in electrical resistivity as shown in Fig. 3.

Up to now, we have discussed the temperature dependence of electrical resistivity, Seebeck coefficient, and power factor. Here, we will discuss the thermal conductivity κ to estimate the ZT and understand the effect of Mn substitution on the ZT. Fig. 6 shows the temperature dependence of κ for x = 0 and 0.4 on a double logarithmic scale. The value of κ increases with the temperature up to about 30 K, and then more or less linearly decreases to 600 K. It is striking that κ of $Mg_{3-x}Mn_xSb_2$ (x = 0.4) is lower than Mg_3Sb_2 (x = 0) below 30 K, but remains the same as that of Mg_3Sb_2 (x = 0) above 30 K. The values at 300 K for both crystals are 1.55 W/mK, which is close to the reported one for polycrystalline Mg_3Sb_2 [11]. As aforementioned, there are two components for κ, namely electron- and phonon-based conductivities. The electronic thermal conductivity κ_{el} can be estimated by the Wiedemann-Franz law, $\kappa_{el} = LT/\rho$, where L is the Lorenz number, and ρ is the electrical resistivity. For non-metallic systems, the lattice thermal conductivity κ_{ph} is dominant, which is related to the structural disorder such as grain boundary and impurity. In an ideal single crystal, the grain boundary effect is negligible. Accordingly, an increase of impurity concentration leads to a decrease in κ_{ph}. In the case of Mg_3Sb_2 system (x = 0), we calculated the κ_{el}, which is negligible due to the large electrical resistivity (see the inset of Fig. 6). As shown in Fig. 6, the κ_{ph} has a dominant role in the temperature dependence of total thermal conductivity. Above 30 K, $\kappa(T)$ is almost identical to each other. This cannot be generally accepted because κ_{ph} should be decreased by Mn impurities which act as impurity scattering center. However, as aforementioned, Mn substitutes for Mg in the tetrahedral site of $(Mg_2Sb_2)^{2-}$ polyanion framework rather than in the octahedral site of Mg^{2+} cation layer, and most phonon heat transfer occurs in the Mg^{2+} cation layer. Therefore, κ is unchanged by the substitution of Mn. Furthermore, we analyze the linear temperature dependence (blue line) above 30 K with the scattering mechanism of phonons. This dependence of κ_{ph} indicates umklapp scattering to be the dominant mechanism in $Mg_{3-x}Mn_xSb_2$ [20].

Finally, we have calculated the figure of merit, ZT (= $S^2T/\rho\kappa$), from the measured electrical resistivity, thermal conductivity, as well as the Seebeck coefficient, and plotted the figure of merit, ZT (= $S^2T/\rho\kappa$) of $Mg_{3-x}Mn_xSb_2$ (x = 0, 0.3, and 0.4) single crystals in Fig. 7 as a function of sample temperature. The ZT for all the single crystals increases as the temperature increases, and the Mn-substituted Mg_3Sb_2 single crystals show much higher ZT than the pure Mg_3Sb_2 single crystal. For example, the ZT for x = 0.4 is almost 20 times higher than that for x = 0 at 300 K. The Mn substitution for Mg is more effective in increasing ZT than other substituted Mg_3Sb_2 [11]. This is because the electrical resistivity is remarkably decreased with the Mn substitution. Furthermore, it is noted that the ZT for the single crystalline Mg_3Sb_2 is much higher than the ZT reported for polycrystalline and nanocrystalline Mg_3Sb_2 [11,12]. The ZT of about 0.11 at 500 K for x = 0.4 is one order of magnitude higher than that for x = 0. This implies that the substitution of Mn for Mg of Mg_3Sb_2 single crystal

can effectively increase the figure of merit, *ZT*, and improve high-temperature thermoelectric properties.

4. Conclusion

Thermoelectric $Mg_{3-x}Mn_xSb_2$ (x = 0, 0.3, and 0.4) single crystals, grown by the vertical Bridgman method, are single phased and *c*-axis oriented with the trigonal crystal structure of inverse α-La_2O_3 type. There are three main conclusions. First, the carrier type of Mg_3Sb_2 is changed from p-type to n-type by introducing Mn. Second, the *ZT* of single crystalline Mg_3Sb_2 is higher than their polycrystalline and nanocrystalline counterparts due to fewer grain boundary scatterings. Third, the *ZT* value is increased by the substitution of Mn and is the largest at x = 0.4, which is the limit of solubility of Mn in $Mg_{3-x}Mn_xSb_2$ phase. Single crystalline $Mg_{3-x}Mn_xSb_2$ could potentially pave the way for improving high-temperature thermoelectric efficiency.

Acknowledgment

This work was supported by the Basic Science Research Program of NRF, the Ministry of Education, Science and Technology of Republic of Korea (South Korea) under Award number 2012R1A1A2039944, and in part by the Sogang University Research Grant of 201310026.01.

References

[1] T. C. Harman, *J. Appl. Phys*., 1958, **29**, 1373.

[2] G. J. Snyder, in *Thermoelectrics handbook: macro to nano*, ed. D. M. Rowe, CRC Press, Boca Raton, FL, 2005, pp. 09/01-09/26.

[3] G. J. Snyder and T. S. Ursell, *Phys. Rev. Lett*., 2003 **91** 148301.

[4] G. J. Snyder and E. S. Toberer, *Nat. Mater*., 2008 **7** 105-114.

[5] H. J. Goldsmid, *Intrdoduction to Thermoelectricity*, Springer, Berlin, Heidelberg, 2010, pp. 23-41.

[6] C. Wan, Y. Wang, N. Wang, W. Norimatsu, M. Kusunoki and K. Koumoto, *Sci. Technol. Adv. Mater*., 2010 **11** 044306.

[7] S. M. Kauzlarich, S. R. Brown and G. J. Snyder, *J. Chem. Soc. Dalton Trans*., 2007 **36** 2099-2107.

[8] E. S. Toberer, A. F. May and G. J. Snyder, *Chem. Mater*. 2010 **22** 624-634.

[9] T. Kajikawa, N. Kimura, T and Yokoyama, Proceedings of the 22nd International Conference on Thermoelectrics, France, 2003, pp. 305-308.

[10] C. L. Condron, S. M. Kauzlarich, F. Gascoin and G. J. Snyder, *J. Solid State Chem*., 2006 **179** 2252-2257.

[11] F. Ahmadpour, T. Kolodiazhnyi and Y. Mozharivskyj, *J. Solid State Chem*., 2007 **180** 2420-2428.

[12] H. X. Xin, X. Y. Qin, J. H. Jia, C. J. Song, K. X. Zhang and J. Zhang, *J. Phys. D: Appl. Phys*., 2009 **42** 165403.

[13] H. X. Xin and X. Y. Qin, *J. Phys. D: Appl. Phys.,* 2006 **39** 5331-5337.

[14] V. Ponnambalam and D. T. Morelli, *J. Electronic Mat*., 2013 **42** 1307-1312.

[15] H. W. Nesbitt and D. Banerjee, *Am. Mineral*., 1998 **83** 305-315.

[16] C. Yilmaz and U. Unal, *J. Electrochem. Soc.,* 2013 **160** 163-167.

[17] H. J. Goldsmid and J. W. Sharp, *J. Electronic Mat*., 1999 **28** 869-872.

[18] G. Busch, F. Hulliger and U. Winkler, *Helv. Phys. Acta*., 1954 **27** 249-258.

[19] T. S. Moss, *Proc. Phys. Soc. (London) B*., 1950 **63** 982-989.

[20] A. Bhardwaj, A. Pajput, A. K. Shukla, J. J. Pulikkotil, A. K. Srivastava, A. Dhar, G. Gupta, S. Auluck, D. K. Misra and R. C. Budhani, *RSC. Adv.,* 2013 **3** 8504-8516.

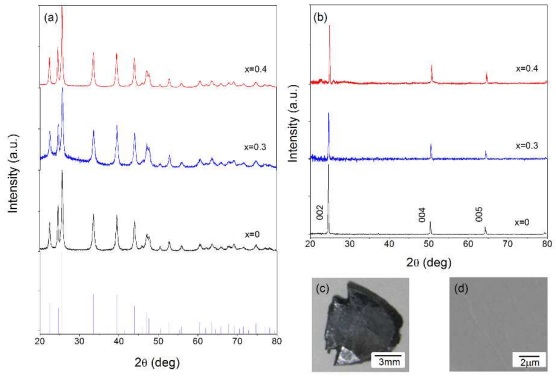

Fig. 1 (a) Powder x-ray diffraction and (b) single-crystal x-ray diffraction patterns for $Mg_{3-x}Mn_xSb_2$ (x = 0, 0.3 and 0.4). The bars represent the reference data of Mg_3Sb_2 with the inverse α-La_2O_3 type structure. (c) Photograph and (d) scanning electron microscope image of single crystal Mg_3Sb_2.

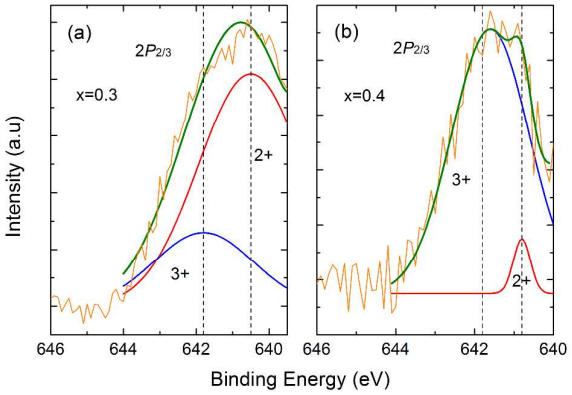

Fig. 2 X-ray photoelectron spectroscopy spectra corresponding to Mn^{2+} and Mn^{3+} binding energies for $Mg_{3-x}Mn_xSb_2$ (x = 0.3 and 0.4). Dashed lines represent the binding energy of $Mn^{3+}(3p_{3/2})$ and $Mn^{2+}(3p_{3/2})$. The blue and red lines are Gaussian functions from $Mn^{2+}(2p_{3/2})$ and $Mn^{3+}(2p_{3/2})$ contributions, and the green line is the sum of them. The yellow line represents the experimental data.

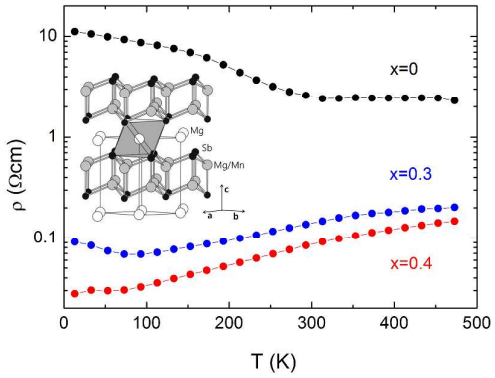

Fig. 3 Temperature dependence of electrical resistivity, ρ for $Mg_{3-x}Mn_xSb_2$ (x = 0, 0.3 and 0.4). Note that the y axis is on a logarithmic scale. The inset represents the schematic crystallographic structure of $Mg_{3-x}Mn_xSb_2$.

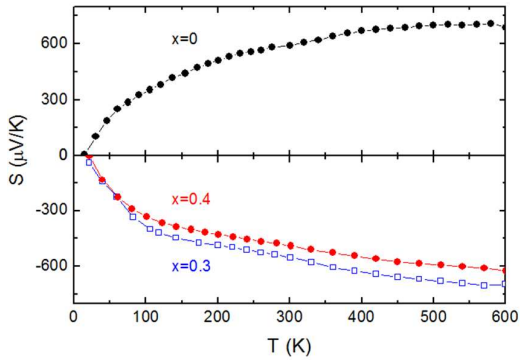

Fig. 4 Temperature dependence of Seebeck coefficient, *S* for $Mg_{3-x}Mn_xSb_2$ (x = 0, 0.3 and 0.4).

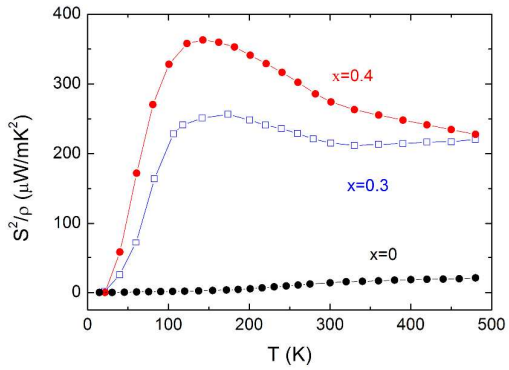

Fig. 5 Temperature dependence of power factor, S^2/ρ for $Mg_{3-x}Mn_xSb_2$ (x = 0, 0.3 and 0.4).

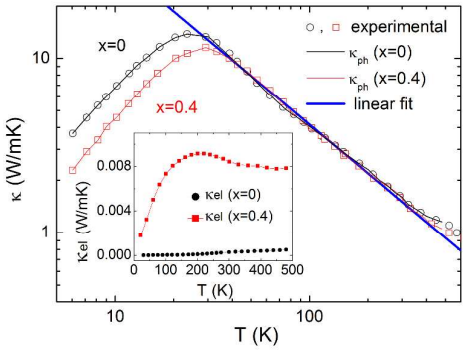

Fig. 6 Temperature dependence of thermal conductivity, κ for $Mg_{3-x}Mn_xSb_2$ (x = 0, 0.4), plotted in a double logarithmic scale. Open symbols represent the experimental data corresponding to the total thermal conductivity, and narrow lines represent lattice thermal conductivity that subtracts the electronic thermal conductivity from the total thermal conductivity. The solid line represents the $1/T$ fit of κ. The inset shows the electronic thermal conductivity that is negligible.

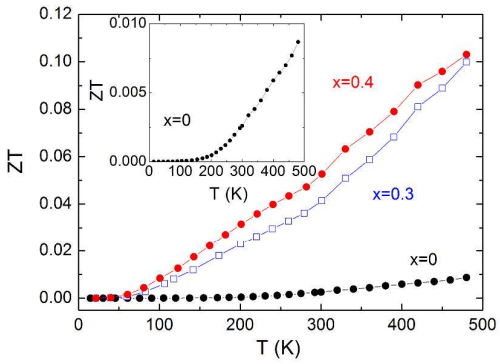

Fig. 7 Temperature dependence of dimensionless figure of merit, *ZT* for $Mg_{3-x}Mn_xSb_2$ (x = 0, 0.3 and 0.4). The inset shows the enlarged plot of *ZT* vs. *T* for x = 0.